Exp. Theo. NANOTECHNOLOGY 10 (2026) 1305-1323 https://doi.org/10.56053/10.3.1305

One-step green synthesis of *Nerium oleander*-capped Fe/Cu bimetallic nanoparticles for high-efficiency adsorption of methylene blue

Wasan Omar Noori, Sama M. Al-Jubouri[*]

Department of Chemical Engineering, College of Engineering, University of Baghdad, Iraq
[*]) Email: sama.al-jubouri@coeng.uobaghdad.edu.iq

Received 21/3/2026, *Received in revised form* 3/4/2026, *Accepted* 25/5/2026, *Published* 15/7/2026

The perpetual release of organic industrial pollutants into the environment increases the aquatic and human health risks. Adsorption technology is an easy and highly effective way for the decontamination of polluted water. In this investigation, Fe/Cu bimetallic NPs are prepared by a green method from the extract of the *Nerium oleander* plant leaf as a stabilizing and reducing agent. The produced bimetallic NPs are examined for their structural features and performance. The characterization results showed that the stabilized hybrid material is quite stable and predominantly amorphous with a mesoporous structure. The surface area, averaged pore diameter, and the pore volume of Fe/Cu bimetallic NPs are found to be 26.07 m^2/g, 14.38 nm, and 0.0937 cm^3/g, respectively. The dye is selected as the simulated contaminant to assess the adsorbent's efficacy in the organic's removal from wastewater. The adsorbent effectively adsorbed 94.2% of the contaminant with a high adsorption capacity of 156.40 mg/g at a primary concentration of methylene blue = 20 mg/L; dose = 0.02 g; solution pH = 10; temperature = 25 °C; mixing time = 130 min. The adsorption process of methylene blue by Fe/Cu bimetallic NPs followed the pseudo-second-order adsorption kinetics and the Freundlich adsorption isotherm. Studying the thermodynamics resulted in negative Gibbs free energy, negative enthalpy, and negative entropy, which means that the adsorption is exothermic, spontaneous, and more ordered.

Keywords: Green synthesis; Fe/Cu bimetallic NPs; Adsorption; *Nerium oleander* leaf extract; Wastewater treatment.

1. INTRODUCTION

A big range of industries, such as textiles, leather, plastics, paper, and even food, use industrial dyes increasingly to meet society's increasing demands [1,2]. The rapid expansion of these companies, coupled with little regulatory monitoring, facilitated the discharge of substantial quantities of dye-contaminated wastewater into aquatic bodies, rendering synthetic dyes a significant source of pollution today [3,4]. These dyes are usually highly water-soluble and possess a complex molecular structure, which makes them refractory to natural degradation in aquatic media [5]. An example is methylene blue (MB; $C_{16}H_{18}ClN_3S$), which is a cationic thiazine dye, applied to dye cellulose-based materials, wood, silk, and cotton. While it is useful in many industrial contexts, MB is an environmental hazard [6] because it is toxic, resistant to natural degradation, and purportedly carcinogenic. The presence of MB's stable aromatic structure further increases its chemical stability, thereby promoting bioaccumulation. This underlines the need for effective removal from wastewater before discharge into natural waters [7]. The physicochemical properties of synthetic dyes make them soluble, stable, and widely distributed even at low concentrations, which makes the conventional treatment technologies ineffective in removing contaminated dyes, thus making the use of alternative technologies a pressing concern [8,9]. A wide variety of physical, chemical, and electrochemical treatment technologies are investigated for dye removal [10,11], including ion exchange, supercritical fluid extraction, membrane separation, electrodialysis, advanced oxidation processes, and electrochemical methods [12-16]. These methods can be good under certain circumstances. Nevertheless, all involve some disadvantages, like high operational costs, high energy consumption, use of hazardous chemicals, long treatment time, and production of secondary pollutants. Hence, their implementation at a large scale has been objectionable [17-23].

Among the technologies developed to date, adsorption has been an efficient method for dye extraction from wastewater. This methodology is highly preferred due to its simple operation, high efficiency, and suitability for diverse adsorbent materials [1,24]. Adsorbents (e.g., zeolites, activated carbon, clay, and metal-organic frameworks (MOFs)) are intensively employed for the adsorptive elimination of such contaminants. On the other hand, adsorbents made from biomass have also attracted a lot of interest for the elimination of such contaminants due to their exceptionally low cost, low environmental impact, and presence of a large extent of surface functional groups [25,26]. In recent years, advances in nanotechnology have enabled the broader use of adsorption systems in wastewater treatment processes [27]. Engineered nanomaterials have stranded as potential adsorbents compared to other adsorbents due to their high adsorption rates as an outcome of their remarkable surface-volume ratios, surface chemistry, and high density of adsorption sites. Nano-metal oxide structures showed a high affinity for adsorbing wastewater contaminants, including dyes, drugs, and heavy metals. This concept is also in line with the current trends of modified nanomaterials that focus on their sustainable applicability [28,29].

In light of the foregoing, iron-based nanoparticles (Fe-based NPs) proved to be efficient nanoadsorbents owing to their magnetic properties and recyclability. Furthermore, the small particle size of the iron-based particles improves mass transfer rates and the availability of reactivity sites, thereby enhancing their adsorption capacity at the solid-liquid interface. Iron-based NPs have also shown potential applicability in the treatment of contaminated wastewater bearing a variety of contaminations such as HM ions, antibiotics, dyes, and others. They showed the ability to adsorb, reduce, complex with, and co-precipitate contaminated materials [28,30]. However, these particles are associated with considerable disadvantages, such as high susceptibility to oxidation and agglomeration, which restrict their adsorption capabilities. Thus, to minimize the disadvantages associated with iron particles, research has focused on incorporating second metal ions such as palladium (Pd), copper (Cu), platinum (Pt), or nickel (Ni) with

iron NPs [31]. The complexes and composites significantly enhance the adsorption capabilities of iron particles. Bimetallic iron particles are mostly associated with the formation of metal synergies that substantially enhance the particle stability. Thereby, the adsorption and catalytic capabilities of the iron NPs are improved, especially for removing dyes, chlorinated compounds, nitrates, heavy metals, and similar components from water systems [31,32]. It is worth mentioning that Iron and copper are abundant, not expensive, and have fewer health effects compared with others.

Conventional synthesis routes of bimetallic Fe-NPs, such as chemical reduction with sodium borohydride, often entail high production costs and the use of toxic substances. Therefore, to address this challenge and provide a solution, cost-effective and ecologically safe approaches to synthesize bimetallic Fe-NPs are among the important subjects, particularly in green chemistry [23,32]. Green synthesis has been confirmed as an easy technique with low toxicity, low cost, and minimal environmental hazards. The natural phytochemicals present in plant extracts act as reducing and stabilizing agents; thus, the use of toxic chemicals and environmental consequences is minimized. Also, the green synthesis provides safer conditions for operation and improved biocompatibility of the synthesized nanoparticles. However, this method may have some limitations, such as the plant's extract composition variation, possible nanoparticles agglomeration, and difficulty in controlling the precise size and morphology of particles. Various plants, including green tea, grape leaves, amaranthus dubius, and eucalyptus, have been successfully used to produce various NPs, including the Fe-NPs [32,33]. Similarly, Cu-NPs are produced using a wide variety of plant extracts, mainly due to the broad applicability of Cu-based nanomaterials in environmental and biomedical sciences. Phytochemicals are present in plant tissue, and they help in reducing metal ions during NPs formation and prevent NPs agglomeration [34,35]. These phytochemicals are also responsible for giving stability in the production of NPs by imparting antioxidant properties, which helps in enhancing the stability of NPs [32,36].

Although there is considerable interest in the application of green-synthesized nanomaterials in wastewater treatment, research in this trend is restricted to monometallic Fe or Cu NPs, with comparably limited research conducted on Fe/Cu bimetallic systems. In particular, the influence of strong reducers, such as plant extracts, on the stability, adsorption, and synthesis of Fe/Cu bimetallic NPs is less investigated. In this context, this study investigates a one-step green synthesis of Fe/Cu bimetallic NPs by *Nerium oleander* plant leaves extract as a strong reducing and stabilizing agent. The properties of the prepared composite will be studied to understand its potential application in wastewater treatment, particularly in MB adsorption. Batch adsorption experiments are conducted to evaluate the adsorption efficiency of the prepared Fe/Cu bimetallic NPs under different operating conditions, including the weight of adsorbent, pH of MB solution, initial dye concentration, temperature, and contact time. Additionally, adsorption kinetics, thermodynamics, and recyclability are investigated.

2. EXPERIMENTAL

2.1 Materials

Ferrous sulfate heptahydrate ($FeSO_4 \cdot 7H_2O$, 98%) and copper sulfate pentahydrate ($CuSO_4 \cdot 5H_2O$, 99%) used as the metal precursors are purchased from BDH, England, and Fluka AG, Switzerland, respectively. Fresh Nerium oleander leaves are collected from Abu Ghraib city, Baghdad, Iraq, and utilized as the plant extract source. MB dye and ethanol (99%) are supplied by Xilong Scientific, China, and utilized without extra purification; all aqueous solutions are made using DI water. The solutions' pH is manipulated by 0.1 M hydrochloric acid (HCl) (98%) obtained from CDH, India, and the same concentration of sodium hydroxide (NaOH) purchased from LTD, India.

2.2 Green preparation of Fe/Cu bimetallic NPs

Fresh *Nerium oleander* leaves are collected and thoroughly washed several times using tap water to clean possible existing dust and impurities. Then, the leaves are rinsed with distilled water to ensure complete cleaning. The washed leaves are air-dried at ambient temperature, finely ground using a mortar and pestle, and finally meshed with a 2.5 mm sieve to obtain a homogeneous powder. For the preparation of the plant extract, 20 g of leaves powder is added to 0.2 L of deionized water (10% w/v). The bulk is initially exposed to ultrasonic treatment at 60 °C for 15 min and subsequently heated to 70 °C for 90 min under continuous stirring. Following cooling the suspension to room temperature, it is subjected to filtration using Whatman No. 1 paper for the removal of the suspended particles. This filtrate is then stored in the refrigerator by keeping it at 4 °C, which will act as a natural stabilizing and reducing agent. Further, the pH of the filtrate is estimated, yielding a value of 0.67.

The fabrication of Fe/Cu bimetallic NPs is performed utilizing a green synthesis method as proposed by Atiya et.al. [32] with margin modifications to optimize the synthesis efficiency. $FeSO_4 \cdot 7H_2O$, weighing 1.39 g, is added to 0.1 L of DI water to give a 0.05 M Fe precursor solution, while $CuSO_4 \cdot 5H_2O$, weighing 0.25 g, is dissolved in 100 mL of DI water to give a 0.01 M Cu precursor solution. The two precursor solutions are then separately subjected to heating and sonication within a water bath that is kept at 60 °C for 15 min. The heating and sonication process ensured the dissolution of the precursors. After this step, the solutions are set together in a 250 mL volumetric flask. Consequently, a homogenous yellow solution, which would be used as a reaction medium in the synthesis process, is obtained. Hence, 75 mL of *Nerium oleander* leaves extract is slowly poured into the homogeneous solution while being stirred to commence the reduction and produce the NPs. After the reaction is complete, the formed nanoparticles are separated by centrifuging at 6000 rpm for 10 min. The precipitated yield is washed with DI water to remove side products, followed by absolute ethanol to clean up the impurities. After washing, an oven is used to dry the product at 80 °C. A schematic clarification of the green fabrication pathway of the Fe/Cu bimetallic NPs is presented in Figure 1.

To investigate the influence of synthesis parameters, additional Fe/Cu bimetallic NPs samples are prepared under identical experimental conditions while varying the Fe: Cu molar ratios (4:1 and 6:1). Table 1 shows regulating the exact Fe: Cu ratios by changing the mass of Fe precursor while keeping the amount of copper salt unchanged. Furthermore, the effect of extract volume is examined using 25 and 50 mL of *Nerium oleander* leaves extract. For comparison, the Fe/Cu bimetallic NPs with a 5:1 molar ratio are also synthesized under a nitrogen atmosphere.

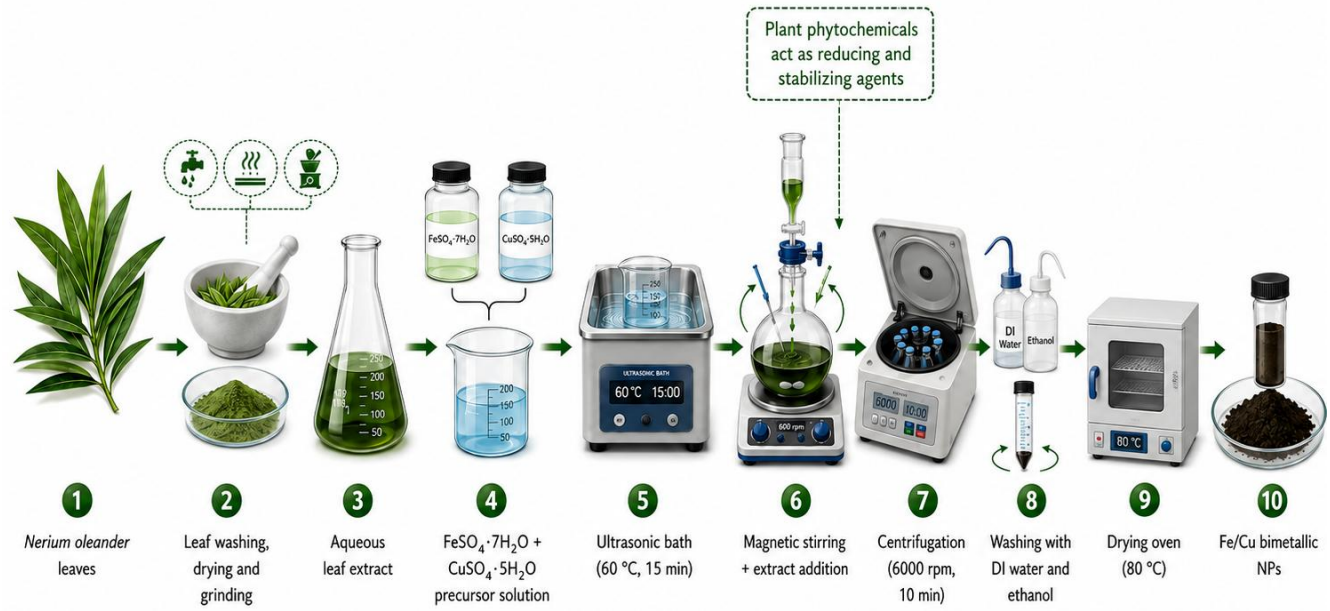

Figure 1 Green synthesis of Fe/Cu bimetallic NPs using *Nerium oleander* leaves.

Table 1 Quantities of metal precursors required for different Fe: Cu molar ratios.

Fe: Cu molar ratio	$FeSO_4 \cdot 7H_2O$ (g)	$CuSO_4 \cdot 5H_2O$ (g)
4: 1	1.112	0.250
5: 1	1.390	0.250
6: 1	1.668	0.250

2.3 Batch adsorption experiments

The synthesized Fe/Cu bimetallic NPs' adsorption toward MB is evaluated in batch experiments. A stock MB solution (50 mg/L) is synthesized by setting 0.05 g of MB dye in 1 L of deionized water, followed by pH control by 0.1 M HCl and/or NaOH when needed. 100 mL of the MB solution is placed into conical flasks, where a predetermined mass of Fe/Cu bimetallic NPs is added. Several operational parameters are varied during the experiments, involving adsorbent dose (0.01-0.03 g/100 mL), solution pH (3-10), original dye concentration (10-30 mg/L), temperature (25-45 °C), and mixing time up to 130 min. For each experiment, an individual factor is varied while all others are fixed. The flasks are shaken using a rotary shaker at 190 rpm for a total contact period of 130 min. At 10 min intervals, samples are taken, centrifuged at 5000 rpm for 5 min, and analyzed at λ_{max} of 664 nm by UV-vis spectroscopy. The adsorption capacity (q_e) and removal ratio are estimated using Equation 1 and Equation 2, respectively.

$$q_e = (C_i - C_e) \times \frac{V}{W} \quad (1)$$

$$\%\, Removal = \frac{C_i - C_r}{C_i} \times 100\% \quad (2)$$

where q_e (mg /g) is the amount (mg) of MB terminated at equilibrium for a specific W (g), which is the mass of a sorbent. V (L) is the MB solution's volume, C_i is the primary concentration of MB, and C_r (mg/L) and C_e (mg/L) are the left concentrations of MB in solutions at a certain time and equilibrium,

respectively. Furthermore, the q_e is denoted by q_t when C_r is substituted in Equation 1, which is measured at various intervals.

To regenerate and reuse the prepared bimetallic NPs, the bimetallic NPs are separated by centrifugation and washed with deionized water several times, followed by ethanol to remove the adsorbed MB. Then, they are overnight dried at 60 °C. The regenerated bimetallic NPs are examined for the adsorption of MB at the best adsorption conditions achieved during the study of the affecting parameters.

2.4 Characterization techniques

X-ray diffraction (XRD) test is conducted by a PHILIPS X-ray diffractometer associated with a Cu anode (Cu Kα radiation, λ = 1.5406 Å), performing at 35 kV and 30 mA. The diffraction patterns are conducted in a 2θ range of 5 to 80° using a step size of 0.04° to evaluate the crystallographic nature of the synthesized Fe/Cu bimetallic NPs. The functional groups and chemical bonds are monitored using a Fourier-transform infrared (FTIR) model Shimadzu IRAffinity-1 spectrophotometer in a scanning range of 4000–400 cm^{-1}. Isotherms of Nitrogen adsorption/ desorption are estimated by a Micromeritics TriStar II Plus surface area and porosity analyzer at 77 K with N_2 as the adsorbate. The Brunauer-Emmett-Teller (BET) approach is adopted to find the surface area, while Barrett-Joyner-Halenda (BJH) and t-plot models are used to find out the pore-size distribution and microporosity. High-resolution Scanning electron microscopy (SEM) is employed to study the morphology and aggregation characteristics of the NPs. The transmission electron microscopy (TEM) pictures are taken using a high accelerating voltage TEM run at 200 kV and coupled with a digital CCD camera. The results are interpreted to understand the primary particle size, shape, and aggregation characteristics of the synthesized Fe/Cu bimetallic NPs. The elemental composition of NPs is checked by energy-dispersive X-ray spectroscopy (EDX), which is coupled with the FE-SEM. The spectra are quantitatively analyzed to understand the elemental composition and weight percentages of the elements present in the synthesized nanoparticles. The NPs surface charge is conducted by measuring their zeta potential by a Malvern Zetasizer Nano ZS equipped with a laser Doppler electrophoresis unit. The sample is dispersed in DI water and analyzed at room temperature. The characterization is performed for Fe/Cu bimetallic NPs with a molar concentration of Fe: Cu = 5:1, synthesized using 75 mL of *Nerium oleander* plant extract under ambient conditions in the absence of nitrogen protection, due to their high adsorption capacity.

3. RESULTS AND DISCUSSION

3.1 Characterization

Figure 2a shows the XRD pattern of Fe/Cu bimetallic NPs synthesized, which exhibited a broad peak over the given range of 2θ. The absence of clear peaks in the XRD confirms that Fe/Cu bimetallic NPs are amorphous in nature. This behavior is usually observed in Fe/Cu bimetallic NPs, which is attributed to strong interactions between Fe/Cu ions and phytochemicals in the plant extract. Another reason is attributed to the organic capping groups on the particle surface, which prevent crystal growth and the development of crystalline structures [37,38]. The TEM image shown in Figure 2b clearly verifies that the size of synthesized NPs varies between 30 and 80 nm, referring to the nanometer-sized nature of the particles. The cloudiness or the interconnected nature of the nanoparticles also verifies the amorphous nature of the particles, as indicated by the XRD pattern. The absence of lattice fringes in the TEM image also verifies the amorphous nature of the formed NPs, rapid nucleation center growth, and a lack of crystalline growth during the green synthesis of nanoparticles. These results are compatible with the reported literature about the synthesis of NPs using a plant extract produced via the green synthesis method [39]. XRD analysis confirmed the amorphous nature of the synthesized Fe/Cu NPs, thereby

preventing accurate estimation of crystallite size. However, TEM images showed particle sizes of 30–80 nm. This difference indicates that the observed particles are mainly amorphous aggregates rather than distinct crystalline domains.

The FTIR spectra of *Nerium oleander* leaf powder and its aqueous extract are presented in Figure 2c, confirming the presence of numerous oxygen- and nitrogen-based groups. The presence of numerous N–H and O–H stretching peaks at around 3414–3422 cm^{-1} confirmed the presence of phenolic, alcoholic, and protein-based compounds. The bands ranging in 2924-2854 cm^{-1} might be assigned to the aliphatic C–H stretching, while the absorption peaks in the range from 1630 to 1070 cm^{-1} are due to carbonyl (C=O), C=C, and C–O stretching. The FTIR spectra confirmed that polyphenolic compounds, proteins, and carbohydrate-based compounds are responsible for the aqueous solution of plant-based leaves. This is documented to play a significant role in the nanoscale green synthesis technique used to reduce metallic salts. The development of Fe/Cu bimetallic NPs using the plant extract significantly changed the FTIR spectrum related to the C=O, O–H, C–O, and C–N stretching. This confirms that plant-based compounds play a big role in reducing Fe/Cu metal salts. The persistence of organic vibrational bands in the nanoparticle spectrum strongly suggests the formation of a phytochemical capping layer, which is crucial in preventing excessive agglomeration and enhancing colloidal stability. In addition, new absorption bands are observed in the low-wavenumber region, particularly around 437 cm^{-1} and near 617 cm^{-1}, which can be appointed to metal-oxygen (Fe-O and/or Cu-O) vibrational modes. Here, spectroscopic evidence for the formation of inorganic Fe/Cu-based nanostructures is provided. It should be noted that FTIR spectroscopy is inherently insensitive to zero-valent metallic bonds (Fe^0 or Cu^0). Therefore, the observed metal-oxygen bands are most likely associated with oxidized or hydroxylated surface layers formed during green synthesis under ambient conditions [40].

The SEM images in Figure 2d reveal that the synthesized Fe/Cu bimetallic NPs form clustered assemblies with predominantly spherical to semi-spherical morphologies. The surface texture is characterized by roughness and porosity, which are characteristics of aggregated nanoparticle structures. Such aggregation is a normal occurrence for nanoparticles produced by green-chemistry synthesis

routes. The organic capping agents used in the synthesis, extracted from the *Nerium oleander* plant, cause aggregation.

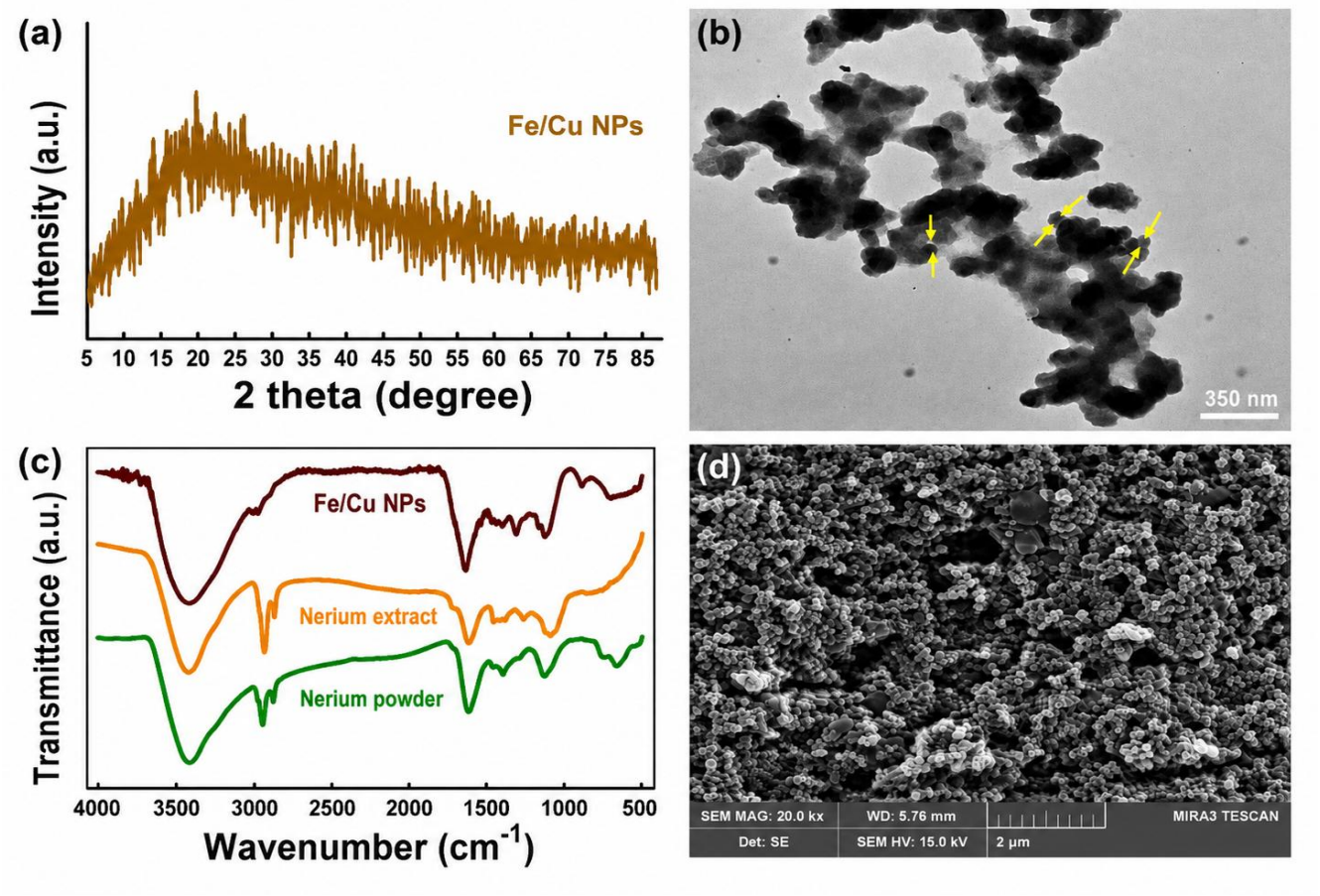

Figure 2 Physicochemical characterization of the green-synthesized Fe/Cu bimetallic NPs, (a) XRD pattern, (b) TEM morphology, (c) FTIR spectrum, and (d) SEM image.

Elemental composition analysis using EDX, illustrated in Figure 3a, indicates the incorporation of iron and copper during nanoparticle synthesis. The weight ratios of the elements identified in the nanocomposite are 54.64% carbon, 37.89% oxygen, 3.81% iron, and 3.66% copper. Although Fe and Cu are identified, the presence of high percentages of carbon and oxygen is due to the presence of other organics found in the plant extract. The identification of Fe and Cu is further proof of the fabrication of iron/copper nanocomposite particles, as proposed earlier [39]. The nitrogen adsorption-desorption isotherm of the Fe/Cu bimetallic NPs exhibits a type-IV profile with an H_3 hysteresis loop, which is characteristic of mesoporous materials composed of aggregated nanoparticles. Textural properties of the fabricated Fe/Cu bimetallic NPs are evaluated using BET analysis. (Figure 3b) The specific surface area is identified as 26.07 m^2/g, with a pore volume of 0.0937 cm^3/g, and a pore diameter of 14.38 nm. These results verify the material's mesoporosity, and the porous structure is favorable for adsorption, promoting mass transfer to active sites for pollutant uptake. The results are consistent with previous work about mesoporous green-synthesized nanomaterials [41]. An excellent colloidal stability is clearly shown by the high zeta potential result of -48.57 mV for the Fe/Cu bimetallic NPs, as depicted in Figure 3c. Stable colloidal systems are characterized by the high magnitude of the zeta potential, i.e., ±30 mV, which enables the minimization of aggregation because of electrostatic repulsions between particles. The

negative charge of the NPs surface can be ascribed to the deprotonated groups of the organic capping generated from plant-based systems, facilitating their stability to be used in water treatment by adsorption [42].

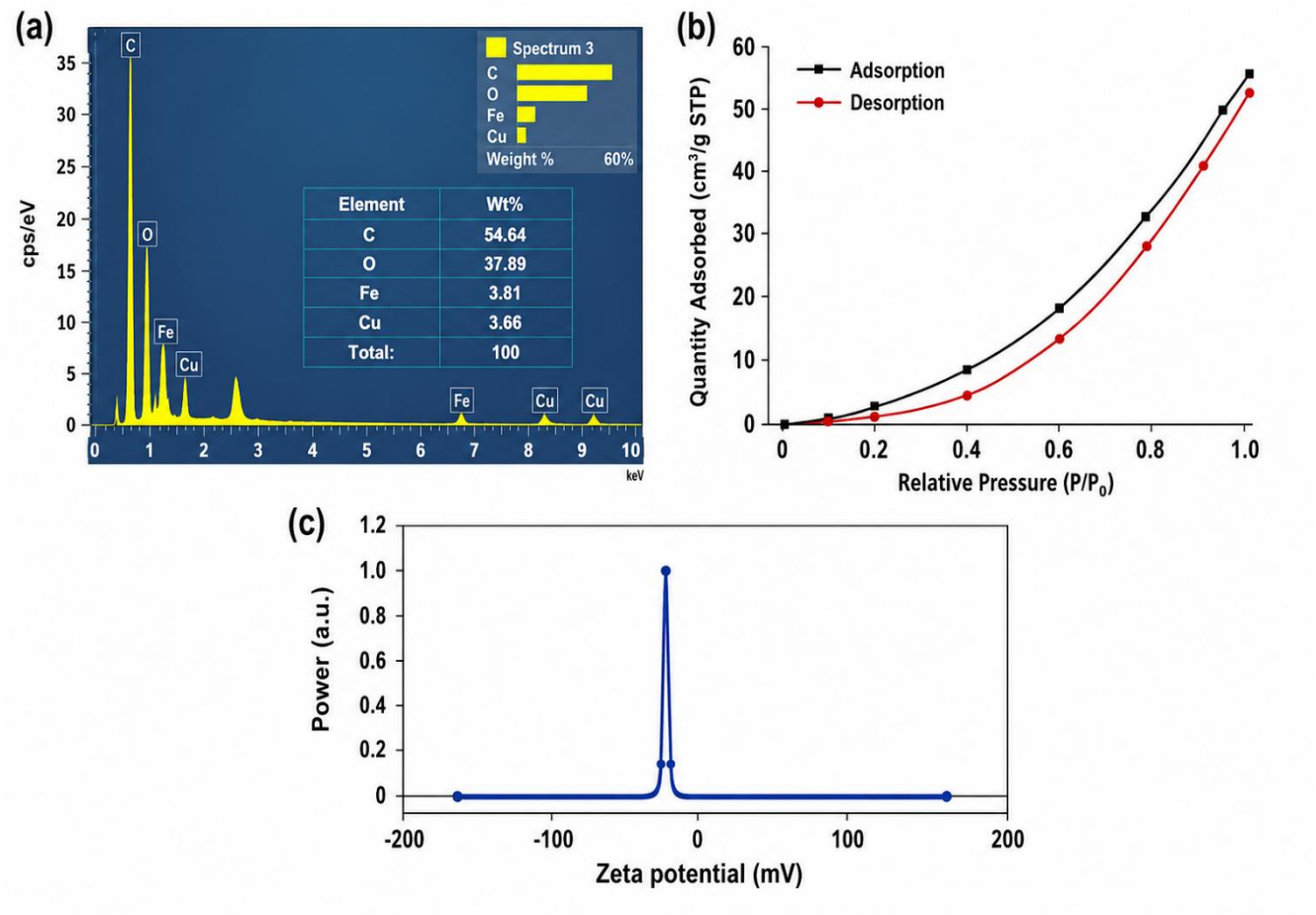

Figure 3 Physicochemical characterization of the green-synthesized Fe/Cu bimetallic NPs, (a) EDX elemental composition, (b) BET adsorption-desorption isotherm, and (c) zeta potential distribution.

3.2 Adsorption performance

3.2.1 Adsorption of NPs synthesized in nitrogen atmosphere

Figure 4a shows the NPs' adsorption performance in a nitrogen atmosphere, compared with that produced in a closed reaction flask without nitrogen. The experimental conditions are 0.02 g Fe/Cu bimetallic NPs/100 mL of 20 mg MB/L and pH = 10 for 130 min at 25 °C. NPs synthesized in the absence of nitrogen are observed to possess a higher adsorption rate and efficiency. NPs synthesized in the absence of nitrogen are observed to remove almost 70% of the dye in the first 20 min. Moreover, the NPs are capable of removing almost 94.2% of the dye in 130 min. However, NPs synthesized in the presence of nitrogen removed only around 60% of the dye in 130 min. Synthesis of NPs in the absence of nitrogen ensures the availability of limited amounts of oxygen. This may facilitate the generation of FeO_x and CuO_x on the surface of the NPs. These oxides may facilitate cationic dye adsorption via electrostatic attraction and complexation.

3.2.2 Impact of Fe to Cu ratio

Figure 4b illustrates the impact of Fe-to-Cu molar ratios on the MB removal efficiency. The experimental conditions are 0.02 g Fe/Cu bimetallic NPs/100 mL of 20 mg MB/L and pH = 10 for 130 min at 25 °C. The NPs synthesized with an Fe:Cu molar ratio of 5:1 exhibited the best performance in the removal of MB, reaching an efficiency of about 94% after 130 min compared to the NPs synthesized with Fe:Cu molar ratios of 4:1 and 6:1. The high efficiency of the NPs synthesized with Fe:Cu molar ratios of 5:1 may be due to the synergistic impacts between Fe and Cu. The moderate Fe content in the NPs may enhance the reactivity of the NPs. The existence of Fe may increase the q_e of the NPs for the cationic dye. The synergistic effects between Fe and Cu may be reduced in the NPs synthesized with Fe:Cu molar ratios of 4:1 and 6:1. The reduced synergistic effects may affect the density of the active sites on the NPs. The effects may change the surface charge merits and the surface morphology of the NPs. The alteration may cause the efficiency of the NPs in the adsorption of the dye to decrease. The results obtained in our work agree with those of Nguyen et. al. [43].

3.2.3 Effect of extract volume

The impact of the volume of the plant extract on the adsorption efficiency of the synthesized bimetallic nanoparticles is presented Figure 4c. This plant extract is utilized as a natural reducing and capping material in the preparation process. The experimental conditions are 0.02 g Fe/Cu bimetallic NPs/100 mL of 20 mg MB/L and pH = 10 for 130 min at 25 °C. As depicted in the figure, the best adsorption efficiency is achieved when the volume of the plant extract is 75 mL, the Fe/Cu bimetallic NPs with a molar concentration of Fe: Cu = 5:1, and under ambient conditions in the absence of nitrogen protection. This led to the best adsorption efficiency of about 94% within 130 min. This high performance can be assigned to the large availability of phytochemicals, such as polyphenols, proteins, and flavonoids. Large extract volume provides more reduction for the biomolecules, which enhances metal ions reduction and improves NPs capping. Also, it leads to smaller particle sizes, surface areas of relatively high values, and higher densities of active sites. Conversely, lower extract volumes (25 mL and 50 mL) limit the amounts of these phytochemicals, resulting in less effective NP formation and reduced adsorption efficiency. This agrees with the previously published study by Nguyen et.al. [43].

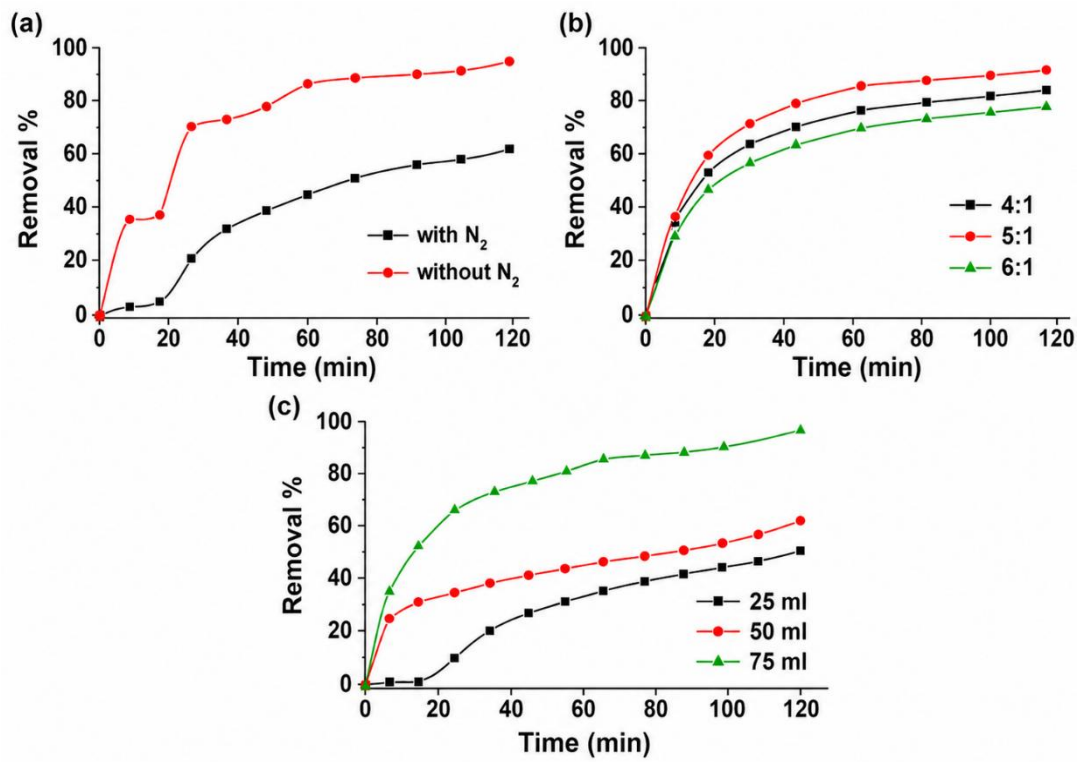

Figure 4 MB removal using Fe/Cu bimetallic NPs a) under nitrogen atmosphere, b) effect of the Fe to Cu ratio, and c) effect of extract volume.

3.2.4 Impact of solution's pH

The initial pH of the solution plays a remarkable role in governing adsorption because it influences the adsorbent's surface charge. The experiments performed at 20 mg/L MB, 0.02 g adsorbent dose, and a temperature of 25 °C demonstrated a clear enhancement in q_e with increasing pH, as presented in Figure 5a. The Fe/Cu bimetallic NPs used in this study exhibited a high negative zeta potential (≈ –48.5 mV), while the MB remained positively charged under almost all tested conditions. At low pH, i.e., pH of 3, the coverage of the NPs surface by H^+ reduced its negative charge, and the competition of the protonated MB with abundant H^+ ions decreased adsorption efficiency. At neutral pH, moderate electrostatic interactions enhanced the adsorption slightly. Higher pH values increased the abundance of hydroxyl groups on the Fe/Cu bimetallic NPs surface, resulting in a more negative charge adsorbent surface and stronger electrostatic attraction toward the cationic MB molecules. This outcome is similar to that reported by El-Maghraby et.al. [44]. Since at alkaline conditions (pH 10), surface functional groups' deprotonation maximized the surface negative charge, leading to the highest removal efficiency. The experimental results showed the MB removal efficiency is 70.6% at pH 3, 76.9% at pH 7, and 94.2% at pH 10. Therefore, pH 10 is selected for the subsequent experimental sections. These observations align with previously reported findings [45,46].

3.2.5 Impact of temperature

Figure 5b shows the impact of temperature (25-45 °C) on MB adsorption. The highest removal efficiency occurred at 25 °C, but it decreased steadily with rising temperature, indicating an exothermic adsorption

process. Strong electrostatic interactions among the MB positively charged molecules and surface groups, negative charge (≡M–O^-) of the Fe/Cu bimetallic NPs dominate at lower temperatures. Increasing temperature enhanced molecular motion, weakening the interactions and reducing the adsorption of MB. The temperature-dependent decrease of the MB removal indicates that the process is mainly controlled by physisorption, where electrostatic and van der Waals forces are sensitive to thermal agitation. High temperatures partially disrupt weak interactions, lowering the uptake of dye molecules. Similar behavior is observed in other oxide-based and green-synthesized nanomaterials [32,47].

3.2.6 Impact of initial dye concentration

MB adsorption is studied at initial concentrations ranging from 10 to 30 mg/L, pH 10, contact time of 130 min, 0.02 g/100 mL of Fe/Cu bimetallic NPs, and at o 25 °C. Figure 5c illustrates that raising the initial concentration resulted in decreased removal efficiency, primarily due to saturating the active sites within the NPs at higher dye loading. The removal efficiency declined from 98.9% to 92.1% for initial MB concentrations of 10-30 mg/L. The removal rate reduced with rising initial concentration, but the q_e increased because of the intensifying driving force of mass transfer. These results indicate that the available active sites become insufficient at higher concentrations, achieving limited adsorption performance. This trend agrees with a previously published study by Ramirez et.al. [48].

3.2.7 Effect of Fe/Cu bimetallic NPs dose

The influence of NPs dosage (0.01, 0.02, and 0.03 g) on the termination of MB dye is tested at a primary dye concentration of 20 mg/L, pH of 10, and room temperature. Figure 5d depicts that the removal efficiency increased progressively with rising NPs dosage due to the abundant availability of active adsorption sites. At 0.01 g, the maximum removal reached approximately 89.5% after 120 min. Increasing the dose to 0.02 g enhanced the removal to about 94.2%, indicating more efficient interaction between MB molecules and the NPs surface. A further increase to 0.03 g resulted in a slight improvement (~99.9%), which may be attributed to particle agglomeration, partial overlap of active sites at higher dosages, and the dimension of the effective surface area [44]. These findings are consistent with an earlier study by Rorissa et.al. [45]. Based on the removal efficiency and material economy, 0.02 g is identified as the best adsorbent dosage.

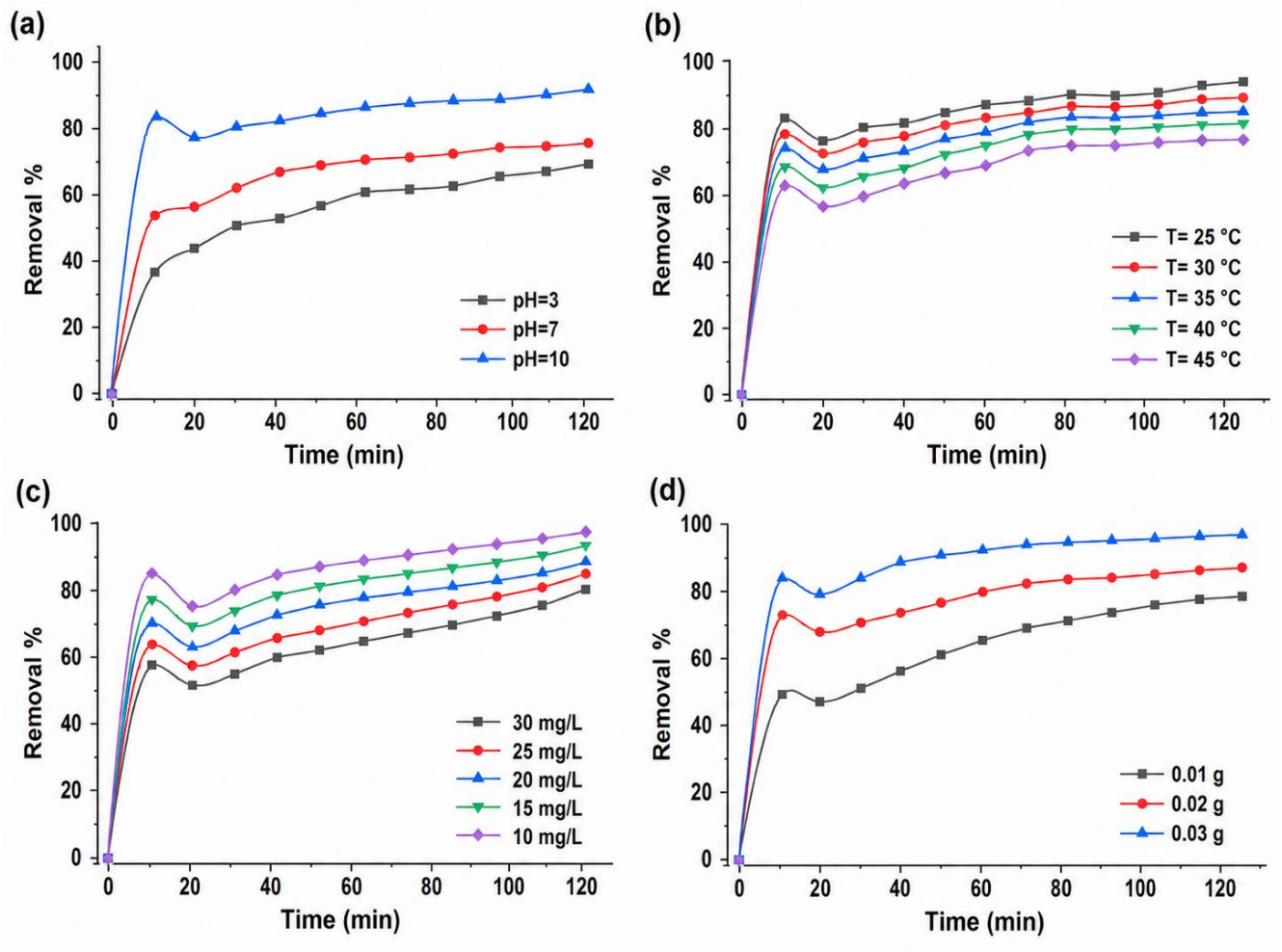

Figure 5 Effect of (a) initial solution pH, (b) initial solution temperature, (c) initial MB concentration, and (d) sorbent dose on the MB removal.

3.3 Kinetic analysis

To facilitate a comprehensive understanding of the adsorption mechanisms and rate-controlling steps for the adsorption process, pseudo-first/pseudo -second-order model, and the Weber-Morris kinetic model are used. In the pseudo-first-order (PFO) kinetic model, the adsorption rate is directly proportional to the concentration of the adsorption sites. In the pseudo-second-order (PSO), the adsorption rate is controlled by the adsorbate-adsorbent interactions, which means the adsorption is a chemisorption containing electron sharing or charge exchange. In the Weber-Morris model, known as the intraparticle diffusion (IPD) kinetic model, the adsorption comprises three stages, namely film diffusion, intraparticle diffusion, and adsorption. The mathematical expressions of these models are presented in Equations 3-5.

$$\ln(q_e - q_t) = \ln q_e - K_1 . t \quad (3)$$

$$\frac{t}{q_t} = \frac{1}{k_2 q_e^2} + \frac{t}{q_e} \quad (4)$$

$$q_t = k_i \cdot t^{0.5} + C_{ip} \quad (5)$$

where q_t (mg/g) denotes the adsorption capacity at any time. The constants k_1 (1/min) and k_2 (g/(mg·min)) are the rate constants of the PFO and PSO models, respectively. For the IPD, ki (mg/(g·$min^{0.5}$)) is the diffusion rate constant, and C_{ip} is a constant referring to the boundary layer effect. Figure 6 shows the kinetics plots of MB sorption.

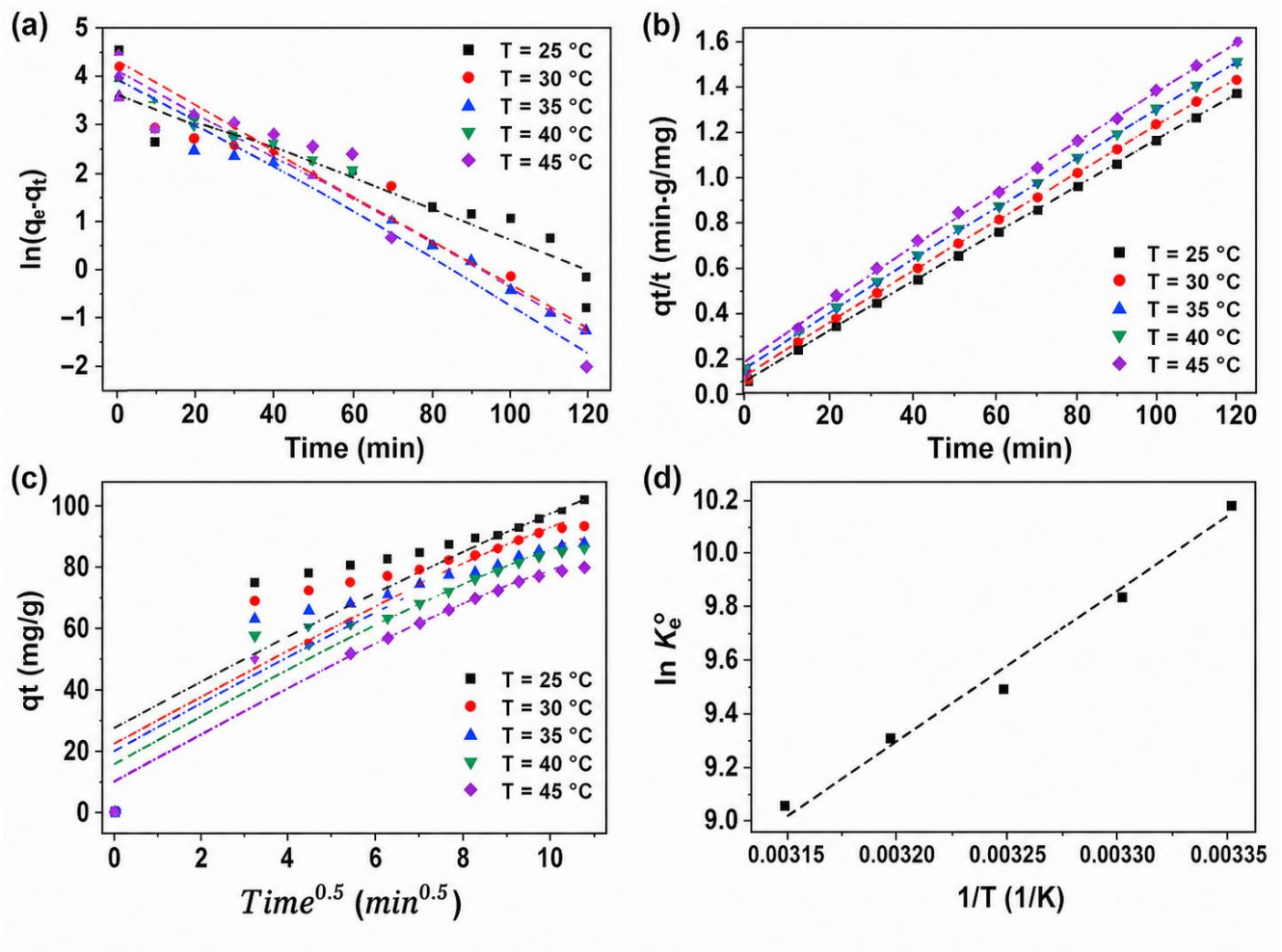

Figure 6 (a) PFO model, (b) the PSO model, (c) the IPD model, and (d) the Van't Hoff plot of MB sorption.

Table 2 Kinetic model parameters for MB adsorption at different solution temperatures.

Model	Parameter	25 °C	30 °C	35 °C	40 °C	45 °C
	q_{exp} (mg/g)	94.205	91.700	88.300	86.500	83.800
PFO	K_1 (min^{-1})	0.033	0.048	0.046	0.049	0.050
	qe (mg/g)	41.380	63.289	51.555	66.193	73.684
	R^2	0.894	0.944	0.959	0.952	0.944
PSO	K_2 (g/mg·min)	0.002	0.0018	0.0021	0.0016	0.0013
	q_e, cal, (mg/g)	97.055	95.720	91.942	91.343	89.579
	R^2	0.999	0.999	0.999	0.998	0.996
IPD	K_i ($mg/g·min^{0.5}$)	5.875	5.9657	5.7301	5.7961	5.7499
	C_{ip} (mg/g)	37.999	35.278	34.369	31.315	28.458
	R^2	0.638	0.677	0.670	0.712	0.743

The estimated parameters based on the applied models are listed in Table 2. The experimental adsorption capacity of MB onto Fe/Cu bimetallic NPs showed excellent matching with the values estimated from the PSO kinetic model at all investigated temperatures, as evidenced by high correlation coefficients (R^2 = 0.996-0.999). This outcome signifies that the process is mainly controlled by chemisorption, in which valence forces via electron sharing or exchange between MB molecules and the NPs' surface-active sites are involved. In contrast, the PFO kinetic model exhibited comparatively lower correlation coefficients (R^2 = 0.894-0.959) and noticeable divergence between the calculated adsorption capacities and the experimentally obtained values. These deviations indicate that the PFO model did not sufficiently represent the adsorption behavior of MB across the whole contact time range, therefore providing a less accurate description of the kinetic mechanism governing this system. To gain a deeper comprehension of the mechanism and potential rate-controlling steps, further investigation is conducted using the IPD model. The plots of q_t versus. $t^{0.5}$ exhibited multi-linear stage behavior with non-zero intercept values (C_{ip}), showing that IPD is not the sole rate-limiting step and that multiple processes contribute to the overall adsorption mechanism. These processes may include rapid adsorption onto the outer surface followed by slower intraparticle diffusion. The results also showed that the boundary layer thickness coefficient (C_{ip}) decreases with increasing temperature, indicating a decrease in external mass transfer resistance. Simultaneously, the IPD constant (K_i) showed only slight variation, demonstrating that temperature influences the diffusion behavior but does not compensate for the noticed decrease in adsorption capacity at higher temperatures. Finally, the kinetic analysis confirms that the adsorption of MB onto Fe/Cu bimetallic NPs is controlled by multiple sequential mechanisms, and chemisorption is the dominant mechanism. Similarly, the PSO kinetic behavior is reported for Fe/Cu bimetallic NPs during MB removal [43,49].

3.4 Isotherm analysis

The equilibrium adsorption characteristics of MB by the synthesized Fe/Cu bimetallic NPs at 25 °C are explored using four basic adsorption isotherm models commonly applied to assess the adsorbent capacities. These adsorption isotherm models include the Freundlich, Langmuir, Dubinin-Radushkevich (D-R), and Temkin. The applicability of the adsorption models provides an explicit understanding of the adsorption mechanism, adsorbent surfaces, and MB molecule interactions with the adsorbent material.

The mathematical forms of the Langmuir, Freundlich, D-R, and Temkin adsorption isotherms are presented in Equations 6-9, respectively.

$$q_e = \frac{q_m.K_L.C_e}{1+K_L.C_e} \quad (6)$$

$$q_e = K_F.C_e^{1/n} \quad (7)$$

$$q_e = q_{DR}.\exp(-\beta\ \varepsilon^2) \quad (8)$$

$$q_e = B.In(A_T.C_e) \quad (9)$$

$$\varepsilon = RT.In\ \left(1+\frac{1}{Ce}\right) \quad (10)$$

$$E = \frac{1}{\sqrt{2\beta}} \quad (11)$$

$$B = \frac{RT}{bT} \quad (12)$$

The Langmuir model describes monolayer uptake on a uniform surface with identical adsorption sites and negligible interactions between neighboring adsorbates. The maximum monolayer capacity (q_m,mg/L) and the Langmuir constant (K_L, L/mg) are obtained to assess adsorption capacity and surface affinity. The Freundlich model represents adsorption on heterogeneous surfaces where multilayer formation of adsorbate may occur. The constants K_F (mg/L.(mg/L)$^{-1/n}$) and n derived from Equation 7 indicate adsorption capacity and intensity, indicating the favorability of dye uptake. To further probe the adsorption mechanism, the D-R model (Equation 8) can be applied, and the Polanyi potential (ε, kJ/mol, Equation 10) is used with the activity coefficient (β, mol^2/kJ^2) to estimate the mean adsorption energy (E, kJ/mol). The E value (Equation 11) is used to distinguish if adsorption is primarily physical or chemical in nature. The Temkin isotherm model works based on the adsorbate–adsorbent interactions and considers a linear reduction in the adsorption heat as the surface coverage increases. The Temkin constants A_T (L/mg) corresponds to the constant of Temkin equilibrium binding, and b_T (J/mol) is related to the variation in adsorption heat. Constant B can be calculated using Equation 12 and reflects the interaction strength between MB molecules and the Fe/Cu bimetallic NPs surface. For consistency in dimensional analysis, SI units must be adopted for C_e (mol/L) and q_e (mol/kg) in the D-R and Temkin isotherm evaluations. The isotherm parameters are obtained from the plots of fitting the experimental equilibrium data to the model's equations.

The curves fitted to the selected isotherm models are illustrated in Figure 7, while the evaluated coefficients are summarized in Table 3. The results showed that the Freundlich model provided the best agreement with the experimental data, registering the highest correlation coefficient (R^2 = 0.955) compared with the Langmuir model (R^2 = 0.935), the D-R model (R^2 = 0.941), and the Temkin model (R^2 = 0.876). This result indicates that the adsorption of MB onto the Fe/Cu bimetallic NPs occurs on a heterogeneous surface, with a possible formation of multiple layers of adsorbed molecules [50]. The Freundlich constant, K_F, which expresses the adsorption capacity, reached a value of 95.22 (mg/g.(mg/L)$^{-1/3}$), indicating a strong affinity between the MB molecules and the Fe/Cu NPs surface. Moreover, the adsorption intensity coefficient (n = 3.10) is > 1, confirming that adsorption is favored within the studied concentration range. The value of n also indicates a relatively strong interaction between the dye molecules and the adsorbent surface, as well as a heterogeneous distribution of the active sites on the surface [51,52]. The Langmuir model also presented good agreement with experimental data, with R^2 of 0.935, which is just below that of the Freundlich model, but it suggests

that the adsorption process simultaneously follows a monolayer mechanism on a homogeneous surface. The highest adsorption capacity estimated by the Langmuir model (q_m = 156.40 mg/g) reflects the high efficiency of the Fe/Cu bimetallic NPs in removing MB dye. The Langmuir constant (K_L = 1.905 L/mg) also indicates a high interaction between the dye molecules and the adsorbent surface [53].

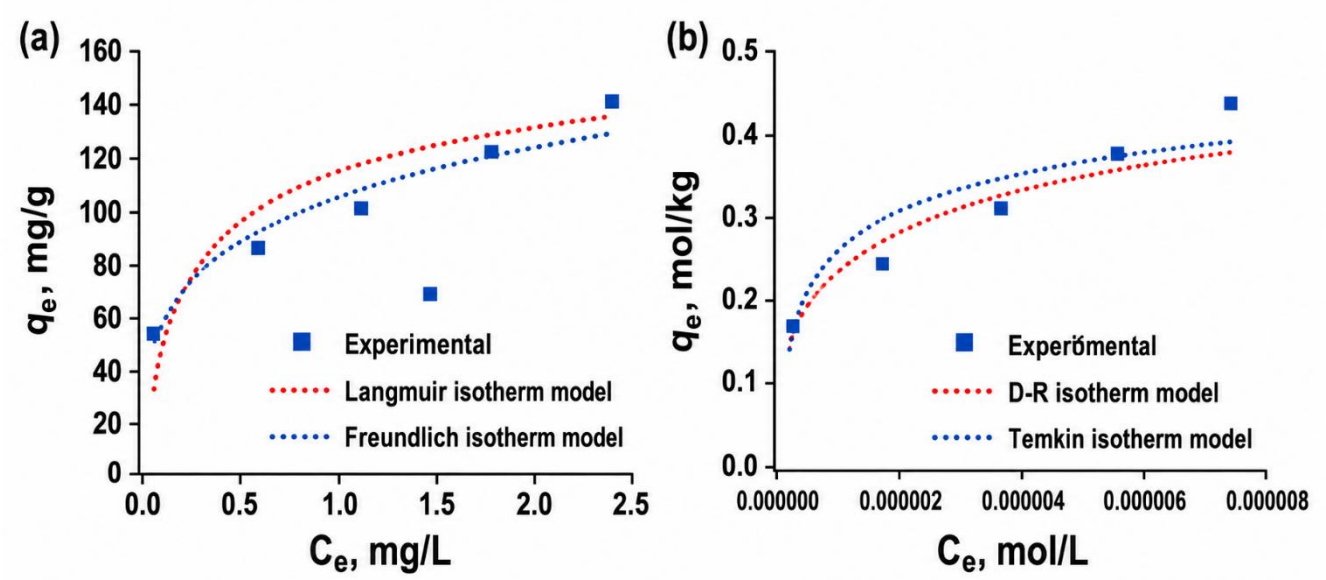

Figure 7 Isotherm models of (a) Langmuir, Freundlich, and (b) (D-R), Temkin for MB sorption by Fe/Cu bimetallic NPs.

Table 3 Summary of isotherm parameters.

Langmuir isotherm model			**Freundlich isotherm model**		
K_L (L/mg)	q_m (mg/g)	R^2	K_F ((mg/g). (mg/L) $^{-1/n}$)	n	R^2
1.905	156.400	0.935	95.220	3.1	0.955
D–R isotherm model			**Temkin isotherm model**		
q_{DR} (mg/g)	E (kJ/mol)	R^2	A_T (L/mole)	b_T (kJ/mol)	B (mole/Kg)	R^2
653.472	16.050	0.941	1.368E+07	29,721	0.083	0.876

The D–R model yielded R^2 of 0.941 and an E of 16.05 kJ/mol. To further illustrate the nature of the adsorption mechanism, the D–R isotherm model is utilized to calculate the mean free energy of adsorption (E). In general, E values lower than 8 kJ mol^{-1} are associated with physisorption mechanisms dominated by van der Waals forces, whereas values between 8 and 16 kJ mol^{-1} indicate ion-exchange or stronger specific interactions. The obtained E value, being close to 16 kJ mol^{-1}, implies that the adsorption of MB onto the Fe/Cu bimetallic NPs involves relatively strong surface interactions. This suggests the participation of specific binding sites and possible surface complexation effects rather than simple physical accumulation of dye molecules. The magnitude of E therefore indicates that the adsorption mechanism possesses a significant specific interaction component, likely related to electrostatic attraction between charged surface sites and dye molecules, as well as possible coordination interactions with surface metal centers. Consequently, the D–R model analysis supports a mechanism

that is more structured and site-dependent than typical physisorption systems [54,55]. The Temkin model, on the other hand, recorded the lowest R^2 value of 0.876, indicating that the heat of adsorption is not uniformly distributed across the surface of the adsorbent. Overall, these results suggest that the adsorption process is best described using the Freundlich model [56].

3.5 Thermodynamic analysis

The thermodynamic parameters are evaluated to elucidate the feasibility and nature of MB adsorption onto Fe/Cu bimetallic NPs at different temperatures. The standard Gibbs free energy change (ΔG°, kJ/mol), enthalpy change (ΔH°, kJ/mol), and entropy change (ΔS°, kJ/mol.K) are found to assess the spontaneity, heat effect, and randomness of the adsorption process. These parameters are calculated using the distribution coefficient (K_q), which is obtained from the equilibrium adsorption capacity and residual dye concentration at each temperature. The thermodynamic parameters are evaluated according to Equations 13-16.

$$\Delta G° = \Delta H° - T\Delta S° \quad (13)$$

$$\Delta G° = -RTlnK_e^{\circ} \quad (14)$$

$$K_q = \frac{q_e}{C_e} \quad (15)$$

$$K_e^{\circ} = \frac{K_q.MW.[Adsorbent]^{\circ}}{\gamma} \quad (16)$$

The combination of Equations (13) and (14) leads to Equation (17).

$$ln\ K_e^{\circ} = -\frac{\Delta H°}{RT} + \frac{\Delta S°}{R} \quad (17)$$

where R is the universal gas constant (8.314 J/mol.K), T is the absolute temperature (K), K_e° is the thermodynamic equilibrium constant (dimensionless), MW represents the molecular weight of the adsorbate, [adsorbate]° represents the adsorbate standard concentration which equals 1 (mol/L), and ɣ is the activity coefficient (dimensionless) and K_q is the distribution coefficient (L/g) found from equation (13). The values of ΔH° and ΔS° are determined from the slope and intercept of the linear Van't Hoff plot of ln K_e° versus 1/T (Figure 6d). The ΔG° values are calculated at each temperature using Equation (13). The calculated thermodynamic parameters are summarized in Table 4.

Table 4 Temperature dependence of K_e°, K_q, and thermodynamic parameters.

T (°C)	T (K)	K_q (L/g)	K_e° (dimensionless)	ln K_e°	ΔG° (kJ/mol)	ΔH° (kJ/mol)	ΔS° (kJ/mol·K)
25	298	81.275	25995.959	10.1657	-25.18	-44.80	-0.066
30	303	55.241	17668.822	9.7796	-24.63		
35	308	37.735	12069.553	9.3984	-24.06		
40	313	32.037	10247.046	9.2347	-24.03		
45	318	25.864	8272.664	9.0207	-23.84		

The negative values of standard free energy (ΔG°) at all studied temperatures confirm that the adsorption of MB onto the Fe/Cu bimetallic NPs is a spontaneous process. The slight decrease in the absolute value of ΔG° with increasing temperature indicates that adsorption becomes less favorable at higher temperatures, suggesting an exothermic process [55]. The negative value of the enthalpy change (ΔH° = -44.8 kJ/mol) further confirms the exothermic nature of the adsorption process and indicates relatively strong interactions between the MB molecules and the active sites on the surface of the Fe/Cu bimetallic

NPs. The magnitude of ΔH° also suggests that the adsorption process may involve strong electrostatic attraction, ion exchange, or at least a chemisorption mechanism [57]. The negative value of the entropy change (ΔS° = -0.066 kJ/mol·K) indicates a decrease in randomness at the solid-solution interface during adsorption, suggesting that MB molecules become more ordered when bound to the Fe/Cu nanoparticle surface [58]. Overall, the thermodynamic parameters confirm that the adsorption process is spontaneous and exothermic, involving strong interactions between the adsorbent surface and the MB molecules.

3.6 Recyclability of Fe/Cu bimetallic NPs

The recyclability profile of the green-synthesized Fe/Cu bimetallic NPs is evaluated over six consecutive adsorption cycles after separation, washing, and drying the used NPs. The experimental conditions are 0.02 g Fe/Cu bimetallic NPs/100 mL of 20 mg MB/L and pH = 10 for 130 min at 25 °C. The initial removal efficiency is 94.2% during the first cycle, which decreased to 90.9%, 89.7%, 87.3%, 85.6%, and 82.2% during the next five cycles, respectively. This predictable decline is commonly attributed to partial surface contamination, progressive occupation of active sites, minor structural adjustments during adsorption–desorption steps, and mass loss during washing between cycles. Despite the gradual decline in adsorption efficiency over successive cycles, the Fe/Cu bimetallic NPs maintained a relatively high removal performance after five regeneration steps, as illustrated in Figure 8. This behavior highlights the structural robustness of the synthesized material and supports its potential for repeated practical application.

The large negative zeta potential value of the Fe/Cu bimetallic NPs, i.e., −48.57 mV, indicates a high electrostatic repulsion among the particles, thereby preventing aggregation during the reuse process. Moreover, the BET results confirm the mesoporous nature of the Fe/Cu bimetallic NPs, with the pore size remaining at 14.37 nm. Finally, the XRD results indicated the presence of an amorphous Fe/Cu matrix, which is likely to provide the Fe/Cu bimetallic NPs with increased structural stability, thus minimizing the likelihood of damage to the structure of the Fe/Cu bimetallic NPs. Overall, the physicochemical properties of the Fe/Cu bimetallic NPs substantiate the recyclability of the Fe/Cu bimetallic NPs synthesized in the study. This is why the Fe/Cu bimetallic NPs retain numerous active adsorption sites even after regeneration. Therefore, the Fe/Cu bimetallic NPs are a promising candidate for the removal of wastewater from contaminated sites.

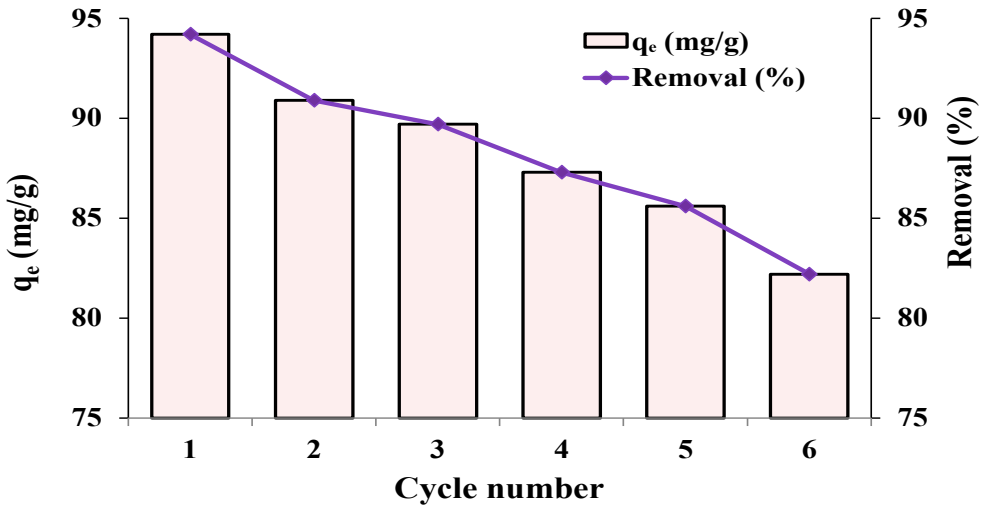

Figure 8 Recyclability of Fe/Cu bimetallic NPs.

3.7 Adsorption mechanism of MB on Fe/Cu bimetallic NPs

Figure 9 illustrates the possible adsorption interactions between MB and the green-synthesized Fe/Cu bimetallic NPs. The adsorption of MB onto green-synthesized Fe/Cu bimetallic NPs is governed by synergistic surface interactions arising from the bimetallic core and the phytochemical capping layer derived from *Nerium oleander* extract. During green synthesis, plant biomolecules introduce abundant oxygen-containing functional groups (-OH, -COOH, and C=O) on the NP surface, rendering it negatively charged under alkaline conditions. Consequently, strong electrostatic attractions occur between the cationic MB molecules and the negatively charged surface sites. Additionally, adsorption is further stabilized by hydrogen bonding between the dye molecules and surface hydroxyl/carbonyl groups, as well as π–π interactions between the aromatic rings of MB and plant-derived phytochemicals [59]. Surface complexation involving the exposed iron and copper active sites enhances MB uptake. In addition, the mesoporous architecture of the Fe/Cu bimetallic NPs promotes efficient diffusion of dye molecules and improves access to the available adsorption sites, thereby contributing to the high adsorption performance [60]. Taken together, the removal mechanism can be attributed to the synergistic contributions of electrostatic attraction, surface complexation, and pore-assisted diffusion, which are characteristic features of green [61,62].

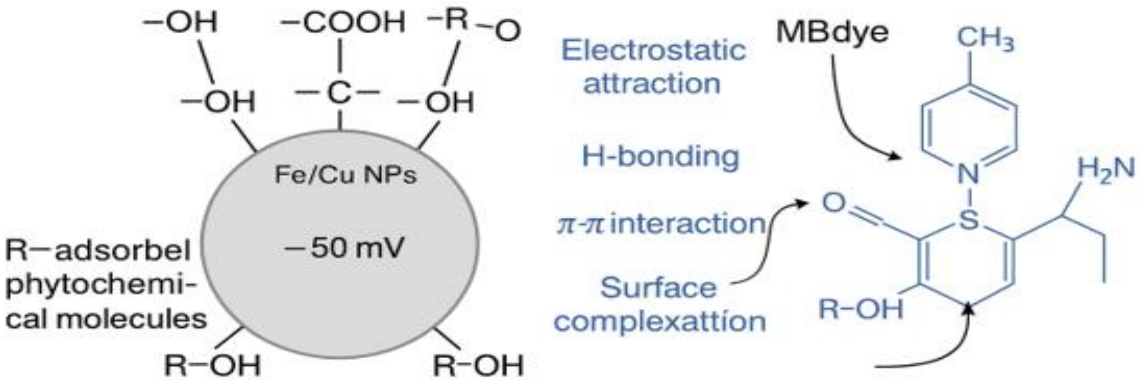

Figure 9 Proposed adsorption mechanism of MB onto green-synthesized Fe/Cu bimetallic NPs.

4. CONCLUSIONS

To sum up the present work, Fe/Cu bimetallic NPs had been effectively synthesized using a green plant-mediated approach with leaf extract of *Nerium oleander* under suitable conditions. For the synthesized Fe/Cu bimetallic NPs, detailed physicochemical characterization had confirmed the formation of amorphous phases with mesopores. Batch adsorption tests showed that the synthesized Fe/Cu bimetallic NPs exhibited high adsorption efficiency for MB under optimal conditions (initial MB concentration = 20 mg/L, adsorbent dose = 0.02 g per 100 mL, solution pH = 10, temperature = 25 °C, and contact time = 130 min). Equilibrium tests showed that the adsorption process by Fe/Cu bimetallic NPs was explained well by the Freundlich isotherm model. Also, the kinetic adsorption tests showed that Fe/Cu bimetallic NPs obeyed the adsorption kinetics of the pseudo-second-order model. This implies that surface effects govern the adsorption process. Thermodynamic evaluation indicated the spontaneous and exothermic adsorption of the MB by the synthesized Fe/Cu bimetallic NPs, involving strong interactions between the adsorbent surface and the MB molecules. The calculated average free energy (E = 16.05 kJ/mol) indicated the presence of strong and relatively specific surface interactions that went beyond simple physical adsorption. In addition, the Fe/Cu bimetallic NPs confirmed a promising candidate for the removal of contamination by keeping 94.2-82.2% of the adsorption efficiency after 6 cycles of reuse.

References

[1] H. Ge, C. Wang, S. Liu, Z. Huang, Bioresour. Technol. 221 (2016) 419 https://doi.org/10.1016/j.biortech.2016.09.060
[2] A. Ayele, D. Getachew, M. Kamaraj, A. Suresh, J. Chem. 2021 (2021) 9923643 https://doi.org/10.1155/2021/9923643
[3] A. Saroa et al., Bioengineered 14 (2023) 1–38 https://doi.org/10.1080/21655979.2023.2260919
[4] A.G. Saleem, S.M. Al-Jubouri, S. Al-Batty, M.W. Hakami, Iraqi J. Chem. Pet. Eng. 26 (2025) 67 https://doi.org/10.31699/ijcpe.2025.1.7
[5] E. Misran, O. Bani, E.M. Situmeang, A.S. Purba, Alexandria Eng. J. 61 (2022) 1946 https://doi.org/10.1016/j.aej.2021.07.022
[6] H.T. Kara, S.T. Anshebo, F.K. Sabir, G.A. Workineh, Int. J. Chem. Eng. 2021 (2021) 9965452 https://doi.org/10.1155/2021/9965452
[7] Z. Peng et al., Nanomaterials 10 (2020) 1560 https://doi.org/10.3390/nano10081560

[8] T. Shindhal et al., Bioengineered 12 (2021) 70 https://doi.org/10.1080/21655979.2020.1863034
[9] A.G. Saleem, S.M. Al-Jubouri, Appl. Sci. Eng. Prog. 17 (2024) 1 https://doi.org/10.14416/j.asep.2024.08.001
[10] J.M. Bidu, K.N. Njau, M. Rwiza, B. Van der Bruggen, S. Afr. J. Chem. Eng. 43 (2023) 112 https://doi.org/10.1016/j.sajce.2022.10.007
[11] A.S. Adday, S.M. Al-Jubouri, S. Al-Batty, Iraqi J. Chem. Pet. Eng. 26 (2025) 19 https://doi.org/10.31699/ijcpe.2025.3.3
[12] S.E.M.E. Mahmoud, D. Ursueguia, M.E. Mahmoud, T.M. Abdel-Fattah, E. Díaz, Biomass Convers. Biorefin. 14 (2024) 19107 https://doi.org/10.1007/s13399-023-04098-9
[13] N.H. Ibrahim, S.M. Al-Jubouri, Iraqi J. Sci. 65 (2024) 6229 https://doi.org/10.24996/ijs.2024.65.11.3
[14] Z. Zhuang, Y. Liu, W. Wei, J. Shi, H. Jin, Biochar 6 (2024) 11 https://doi.org/10.1007/s42773-024-00302-9
[15] S.M. Al-Jubouri, S. Al-Batty, R.K.S. Al-Hamd, R. Sims, M.W. Hakami, S.K.M. Haque, Asia-Pac. J. Chem. Eng. 18 (2023) 1 https://doi.org/10.1002/apj.2941
[16] E.M. Khudhair, Y.S. Kareem, S.H. Ammar, A.S. Mahdi, Mater. Today Proc. 120 (2026) 41 https://doi.org/10.1016/j.matpr.2023.04.058
[17] M.A. Mohammed, W.O. Noori, H.A. Sabbar, Iraqi J. Chem. Pet. Eng. 21 (2020) 39 https://doi.org/10.31699/IJCPE.2020.3.5
[18] A.A. Beddai, B.A. Badday, A.M. Al-Yaqoobi, M.K. Mejbel, Z.S. Al Hachim, M.K.A. Mohammed, Int. J. Chem. Eng. 2022 (2022) 4713399 https://doi.org/10.1155/2022/4713399
[19] N.H. Ibrahim, S.M. Al-Jubouri, A. Alfutimie, Iraqi J. Chem. Pet. Eng. 24 (2023) 27 https://doi.org/10.31699/ijcpe.2023.3.3
[20] D.D.H. Rio, S.M. Al-Jubouri, S.M. Holmes, Chim. Oggi - Chem. Today, 35 (2017) 26
[21] A.S. Adday, S.M. Al-Jubouri, Case Stud. Chem. Environ. Eng. 10 (2024) 100852 https://doi.org/10.1016/j.cscee.2024.100852
[22] A.S. Mubarak, S.S. Salih, M. Kadhom, T.K. Ghosh, Sustain. Chem. Environ. 9 (2025) 100231 https://doi.org/10.1016/j.scenv.2025.100231
[23] M.A. Asghar et al., LWT 90 (2018) 98 https://doi.org/10.1016/j.lwt.2017.12.009
[24] J. Yang, S. Shojaei, S. Shojaei, npj Clean Water 5 (2022) 1 https://doi.org/10.1038/s41545-022-00148-3
[25] R. Agarwala, L. Mulky, ChemBioEng Rev. 10 (2023) 326 https://doi.org/10.1002/cben.202200011
[26] F. Pirvu, C.I. Covaliu-Mierlă, G.A. Catrina, Nanomaterials 13 (2023) 1745 https://doi.org/10.3390/nano13111745
[27] A. Mohammadpour et al., Environ. Res. 225 (2023) 115507 https://doi.org/10.1016/j.envres.2023.115507
[28] S. Rezania, N. Darajeh, P.F. Rupani, A. Mojiri, H. Kamyab, M. Taghavijeloudar, Appl. Sci. 14 (2024) 11492 https://doi.org/10.3390/app142411492
[29] H.S. Alshehri, Pol. J. Environ. Stud. Online First (2025) https://doi.org/10.15244/pjoes/205261
[30] M.M.A. Aslam et al., Sustain. Mater. Technol. 44 (2025) e01362 https://doi.org/10.1016/j.susmat.2025.e01362
[31] M.M. Abdul Hassan, S.S. Hassan, A.K. Hassan, Eurasian Chem. Commun. 4 (2022) 1062 https://doi.org/10.22034/ecc.2022.342067.1466
[32] M.A. Atiya, A.K. Hassan, I.M. Luaibi, Nat. Environ. Pollut. Technol. 21 (2022) 355 https://doi.org/10.46488/NEPT.2022.v21i01.043
[33] X. Weng, M. Guo, F. Luo, Z. Chen, Chem. Eng. J. 308 (2017) 904 https://doi.org/10.1016/j.cej.2016.09.134

Exp. Theo. NANOTECHNOLOGY 10 (2026) 1305-1323
[34] H.C.A. Murthy, T. Desalegn, M. Kassa, B. Abebe, T. Assefa, J. Nanomater. 2020 (2020) 3924081 https://doi.org/10.1155/2020/3924081
[35] M. Fazlzadeh, K. Rahmani, A. Zarei, H. Abdoallahzadeh, F. Nasiri, R. Khosravi, Adv. Powder Technol. 28 (2017) 122 https://doi.org/10.1016/j.apt.2016.09.003
[36] K.A.P. Gaminda, I.B.K. Thomas, P. Lakmauri, T. Abeysinghe, C. Jayasinghe, R. Senthilnithy, Environ. Nanotechnol. Monit. Manag. 21 (2024) 100925 https://doi.org/10.1016/j.enmm.2024.100925
[37] G. Zhang et al., J. Hazard. Mater. 398 (2020) 122889 https://doi.org/10.1016/j.jhazmat.2020.122889
[38] J. He et al., J. Environ. Chem. Eng. 11 (2023) 109877 https://doi.org/10.1016/j.jece.2023.109877
[39] S.-K. Chen, P.-H. Lee, H. Lee, H.-T. Su, Mater. Chem. Phys. 210 (2018) 336 https://doi.org/10.1016/j.matchemphys.2017.08.008
[40] E. Valle-Rivera et al., Crystals 15 (2025) 226 https://doi.org/10.3390/cryst15030226
[41] Q. Feng, X. Tai, Y. Sun, M. Li, Chem. Eng. J. 378 (2019) 122123 https://doi.org/10.1016/j.cej.2019.122123
[42] F. Besharat, F. Ahmadpoor, M. Nasrollahzadeh, J. Mol. Liq. 334 (2021) 116123 https://doi.org/10.1016/j.molliq.2021.116123
[43] H.S. Nguyen, V.H. Nguyen, T.T.H. Nguyen, N.T. Vu, N.H. Le, Nano Express 5 (2024) 025026 https://doi.org/10.1088/2632-959X/ad5221
[44] A. El-Maghraby, H.E. El Deeb, Glob. NEST J. 13 (2011) 90 https://doi.org/10.30955/gnj.000560
[45] G.L. Rorissa et al., Sci. Rep. 15 (2025) 26230 https://doi.org/10.1038/s41598-025-11746-9
[46] A. Nasser, S. Kareem, Wasit J. Eng. Sci. 11 (2023) 94 https://doi.org/10.31185/ejuow.Vol11.Iss2.466
[47] J.B. Adeoye et al., Discov. Appl. Sci. 7 (2025) 1285 https://doi.org/10.1007/s42452-025-07250-4
[48] L. Ramirez, P. Le, S. Ramseier, Sci. Total Environ. 856 (2023) 159261 https://doi.org/10.1016/j.scitotenv.2022.159261
[49] T. Shahwan, M. Anjass, R. Naser, J. Mater. Environ. Sci. 12 (2021) 42
[50] U. Isah, M. Abdullahi, H. Abdul-Hamid, J. Mater. Environ. Sci. 15 (2024) 893
[51] M.A. Ahmad, M.F.M. Yusop, R. Zakaria, J. Karim, N.K.E.M. Yahaya, M.A.M. Yusoff, N.H.F. Hashim, N.S. Abdullah, Mater. Today Proc. 47 (2021) 1246 https://doi.org/10.1016/j.matpr.2021.02.789
[52] A.A. Fakunmoju, F. Azaman, S. Hamzah, A. Ali, Lett. Appl. NanoBioSci. 14 (2025) 144 https://doi.org/10.33263/LIANBS143.144
[53] H.R. Yuliani, A. Musfirah A., I.A.N.P.Z. Isma, I.A.I. Adriani, H. Setiawati, Proc. iCAST-ES 2021 (2023) 800 https://doi.org/10.5220/0010953900003260
[54] M.A. Abduljabar, Ibn Al-Haitham J. Pure Appl. Sci. 37 (2024) 264 https://doi.org/10.30526/37.3.3398
[55] N.H. Ibrahim, S.M. Al-Jubouri, Asia-Pac. J. Chem. Eng. 19 (2024) e2967 https://doi.org/10.1002/apj.2967
[56] B.T. Danat, W.R. Ahulle, H.F. Chahul, I.M. Saviour, Appl. Water Sci. 16 (2026) 72 https://doi.org/10.1007/s13201-025-02682-0
[57] S. Davoudi, Iran. J. Chem. Chem. Eng. 41 (2022) 2343 https://doi.org/10.30492/ijcce.2021.526904.4630
[58] J. Zhang, G. Zhang, Q. Zhou, L. Ou, J. Water Reuse Desal. 6 (2016) 301 https://doi.org/10.2166/wrd.2015.121
[59] H.M. Abuzeid, C.M. Julien, L. Zhu, A.M. Hashem, Crystals 13 (2023) 1576 https://doi.org/10.3390/cryst13111576
[60] R.A. Rasheed, M.F.A. Alias, Exp. Theo. NANOTECHNOLOGY 10 (2026) 69 doi:10.56053/10.1.69

[61] A.Q. Tuama, G.A. Fadhil, W.A.S. Al-dulaimi, Exp. Theo. NANOTECHNOLOGY 10 (2026) 25 doi:10.56053/10.1.25
[62] H.A. Sabbar, W.O. Noori, A.S. Naje, Pertanika J. Sci. Technol. 28 (2020) 353 https://doi.org/10.47836/pjst.28.1.24